IEEE Access
Multidisciplinary | Rapid Review | Open Access Journal

Received November 7, 2019, accepted November 20, 2019, date of publication November 25, 2019,
date of current version December 13, 2019.

Digital Object Identifier 10.1109/ACCESS.2019.2955605

Signal Detection Based on Second-Order Underdamped Tristable Stochastic Resonance and Its Application to Weak Fault Diagnosis

WENYUE ZHANG[1], PEIMING SHI[1], MENGDI LI[1], YONGXU JIAO[1], AND DONGYING HAN[2]

[1]School of Electrical Engineering, Yanshan University, Qinhuangdao 066004, China
[2]School of Vehicles and Energy, Yanshan University, Qinhuangdao 066004, China

Corresponding author: Peiming Shi (spm@ysu.edu.cn).

This work was supported in part by the National Natural Science Foundation of China under Grant 61973262 and Grant 51875500, and in part by the Natural Science Foundation of Hebei Province under Grant E2019203146 and Grant E2015203190.

ABSTRACT The advantages of stochastic resonance (SR) have received extensive attention and research in the field of weak signal extraction. It can be used to extract fault signals from rotating machinery. To deeply improve the output signal-to-noise ratio (SNR), a second-order underdamped tristable stochastic resonance (SUTSR) is proposed in the present study. The potential function, the steady-state probability density of particles and the SNR are used to evaluate the model. Firstly, the relationship between the noise intensity and the SNR of SUTSR is studied. Then, using the steady-state solution curve, the output response of the SUTSR system is discussed from the perspective of steady-state input, and the output response of the system is further studied when inputting low-frequency harmonic signals. Finally, SUTSR model is used to process bearing signal data with inner ring fault and rolling element fault, and the processing result is compared with tristable system and second-order underdamped bistable system. The results show that, in the background of strong noise, the SUTSR system can accurately identify the characteristic frequency of the fault signal and then greatly improve the energy of the weak fault signal under appropriate system parameters.

INDEX TERMS Stochastic resonance, second-order, tristable system, damping factor, SNR.

I. INTRODUCTION

Stochastic resonance is a nonlinear system containing characteristic signals and noise. Under suitable conditions, the injected noise instead causes the intensity of the output signal to exhibit a gain change. Benzi *et al.* [1], [2] firstly proposed the concept of stochastic resonance. Since then, the researchers have not only observed the phenomenon of stochastic resonance in the experiment [3], but also constantly proposed a new theory of stochastic resonance. For more than 30 years, the concept of stochastic resonance has been extensively appeared in many subjects such as meteorology [4], optoelectronics [5], [6], biomedicine [7], [8], and mechanical mechanics [9]–[12]. In recent years, researchers have paid great attention to the field of stochastic resonance and have yielded substantial results in the process of detecting the weak signal [13]–[15]. The one-dimensional Langevin equation model driven by weak signals and noise is the most classical stochastic resonance model [16]. In recent years, new stochastic resonance models have been proposed, such as monostable systems, multi-stable systems, time delay systems, chaotic systems, and two-dimensional Duffing systems [17]–[19]. These models greatly enrich the theory of stochastic resonance and extend the application of stochastic resonance. Since the multi-stable system and the underdamped system are particularly prominent in the filtering ability, they have attracted the attention of many researchers. However, few researchers have focused on underdamped multi-stationary stochastic resonance systems.

Extensive research stochastic resonance in mechanical fault diagnosis has been applied. Hu et al. proposed an improved SR method for machine signal processing [20]. Nishiiguchi K et al. demonstrated that bistable stochastic resonance of nano field effect transistors can detect those weak signals submerged in noise [21]. Li et al. proposed a second-order bistable stochastic resonance model based on wavelet transform, which successfully realized the extraction of weak fault characteristics in wind turbine

The associate editor coordinating the review of this manuscript and approving it for publication was Yue Zhang.

vibration signals [22]. Lai et al. studied the dynamic response of tristable SR system [23], [24]. Xu et al. studied the mechanism of underdamped tristable SR by deriving the SNR and the average first crossing time [25]. The effects of time-delayed term as well as noise on SR systems were focused on by Wang *et al.* [26], [27]. By adopting the adaptive stochastic resonance, Yang et al. improved the bearing fault diagnosis efficiency and at the same time they used a new stochastic resonance method to recover an unknown signal entirely submerged in strong noise [28], [29]. He et al. conducted a study on the measure of stochastic resonance and proposed to use statistical complexity to quantify the stochastic resonance system [30], [31]. Duan et al. investigated the noise benefits to maximum likelihood type estimators to make a robust estimation to a location parameter [32].

Since the classical stochastic resonance model is an over-damped first-order differential equation, which means that the inertial term of the system is ignored, so the damping factor is normalized. However, the output of SR is the trajectory of Brownian particles in the potential well, so the inertia term and damping of the system will affect the state of stochastic resonance. When considering the inertial term of the system, the stochastic resonance model becomes a second-order stochastic differential equation. Lu et al. studied the application of underdamped variable step size second-order SR algorithm in fault diagnosis [33]. Dong et al. studied the effects of second-Order matched stochastic resonance to detect weak signal [34]. He et al. proposed a combination of adaptive second-order stochastic resonance and modal decomposition to detect bearing signals with early faults [35]. In terms of signal processing, the output of the underdamped system equation is equivalent to the secondary filtering, so the second-order stochastic resonance model has a better filtering effect on signal processing. At the same time, it is well known that multi-stable systems have also been widely studied by scholars because of their excellent filtering effects. However, little attention has been paid to multi-stable systems based on underdamping. No one has explored the effect of the model on actual signal processing.

This paper proposes a second-order underdamped tristable SR system and further discusses whether it is feasible to extract weak fault signature in the system. In Section 2, the system model is given and the generalized potential function, steady-state probability density and output SNR are derived. And then the intrinsic influence of system parameters on the model is studied. In Section 3, the steady-state solution curve is introduced and the output response of the SUTSR system under harmonic excitation is analyzed. In Section 4, the performance of the SUTSR model is tested with actual data and compared with other stochastic resonance methods. Finally, Section 5 draws some conclusions.

II. SYSTEM MODEL

A. THEORETICAL BACKGROUND

British botanist Brown discovered in 1827 that under the impact of water molecules, the movement of pollen particles showed strong irregularities, which is known as Brownian motion. Later, based on this theory, Langevin proposed an equation for describing the irregular motion of particles Langevin Equation (LE):

$$m\frac{\mathrm{d}^2x}{\mathrm{d}t^2} = -\lambda\frac{\mathrm{d}x}{\mathrm{d}t} + F(t) \tag{1}$$

where m is the mass of the Brownian particle, x is displacement, $-\lambda \mathrm{d}x/\mathrm{d}t$ is the resistance of liquid to particles, $F(t)$ is the noise force generated by an irregular collision. Random noise has a Gaussian probability distribution with a mean of 1 and a variance of 0. When ignoring gravity and other external forces, Eq. (1) can be rewritten as:

$$\frac{\mathrm{d}^2x}{\mathrm{d}t^2} = -\gamma\frac{\mathrm{d}x}{\mathrm{d}t} + \xi(t) \tag{2}$$

where $\gamma = \lambda/m$, $\xi\ (t) = F(t)/m$

Noise can be used to enhance weak periodic signals under suitable conditions. After the Langevin equation was proposed, Benzi et al. used the Langevin equation to model the underdamped stochastic resonance:

$$\mathrm{d}x = \left[x\left(a - x^2\right)\right]\mathrm{d}t + \varepsilon \mathrm{d}w(t) \tag{3}$$

where $w(t)$ is the wiener process. The solutions of Eq. (2) Which are $x_{1,2} = \pm\sqrt{a}$ and $x = 0$. Under the effect of small periodic force, the Eq. (3) becomes:

$$\mathrm{d}x = \left[x\left(a - x^2\right) + A\cos\omega t\right]\mathrm{d}t + \varepsilon \mathrm{d}w(t) \tag{4}$$

When the noise intensity is appropriate ($\varepsilon \in (\varepsilon_1, \varepsilon_2)$), Eq. (3) will have an output with the same period as the small period force. But the amplitude of the output increases to $2\sqrt{a}$.

B. SECOND-ORDER UNDERDAMPED TRISTABLE STOCHASTIC RESONANCE SYSTEM (SUTSR)

It can be inferred from the above analysis that the classical stochastic resonance uses an overdamped first-order stochastic differential equation, which means that the inertial term in the original LE is ignored. In fact, when we think that the output of SR is the trajectory of the particle in the potential well, the inertia and damping of the system will affect the realization of SR.

According to the Brownian motion and LE of Section 2.1, we consider both the damping coefficient and the inertia term for the SR system model. A second-order underdamped stochastic resonance system based on multi-stable can be defined as:

$$\frac{\mathrm{d}^2x}{\mathrm{d}t^2} + \frac{\mathrm{d}U\ (x)}{\mathrm{d}t} + \gamma\frac{\mathrm{d}x}{\mathrm{d}t} = S\ (t) + \eta(t) \tag{5}$$

where $S\ (t) = A\cos\ (2\pi ft + \varphi)$ is the input periodic signal, in which A represents the amplitude, f represents the driving frequency and φ represents the phase. $\eta\ (t) = \sqrt{2D}\xi(t)$ is Gaussian white noise (zero mean, unit variance). γ represents

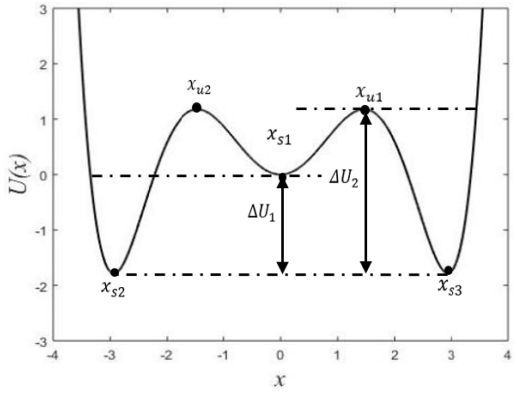

FIGURE 1. The multi-stable potential function $U(x)$.

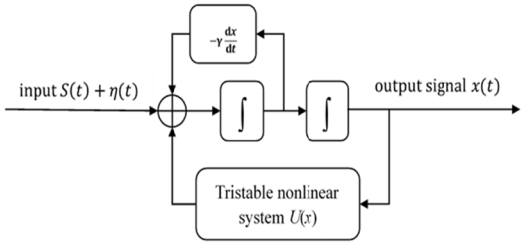

FIGURE 2. The system model of the underdamped second-order SR based on tristable.

the system damping factor. $U(x)$ is a tristable potential well can be represented as follows:

$$U(x) = \frac{b}{2}x^2 + \frac{c}{4}x^4 + \frac{d}{6}x^6 \tag{6}$$

where b, c, and d are system parameters.

According to Eq. (2), the potential function $U(x)$, as shown in Fig. 1, is symmetrical and has three stable points and two potential barriers.

Substitute Eq. (6) into Eq. (5), then the following equation can be written as:

$$\frac{\mathrm{d}^2x}{\mathrm{d}t^2} = -bx - cx^3 - dx^5 - \gamma\frac{\mathrm{d}x}{\mathrm{d}t} + A\cos(2\pi ft + \varphi) + \sqrt{2D}\xi(t) \tag{7}$$

The system model of Eq. 7 is shown in Fig. 2. It can be deduced that the output of SUTSR is a secondary integral output process. At the same time, the integration process can be equal to the low-pass filtering process. So, the SUTSR system will greatly improve the output SNR compared with the general first-order system.

Fig. 3 shows the motion of Brownian particles subjected to periodic driving forces in a multi-stationary well. The potential well contains three steady-state points and two non-steady-state points. The Brownian particles are driven by the driving force from the leftmost potential well to the rightmost potential well, and finally return to the left potential well to complete a cycle of motion.

C. SIGNAL TO NOISE RATIO (SNR) ANALYSIS

In order to facilitate the calculation, we make $\gamma = 0$, $\varphi = 0$, and $\frac{\mathrm{d}x}{\mathrm{d}t} = y$, and then we transform the second-order system

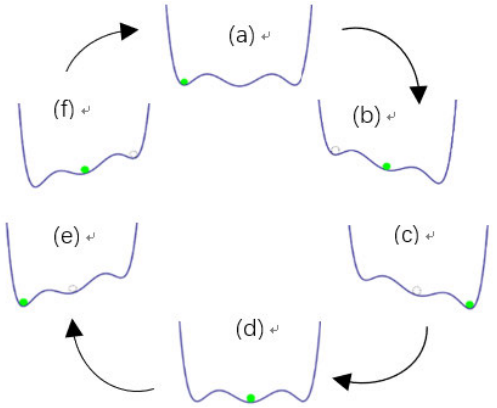

FIGURE 3. State transition of the tristable system in the presence of periodic force and noise.

of Eq. (7) into the first-order system, which can be defined as:

$$\begin{cases} \dfrac{\mathrm{d}x}{\mathrm{d}t} = y \\ \dfrac{\mathrm{d}y}{\mathrm{d}t} = -bx - cx^3 - dx^5 \\ \qquad + A\cos(2\pi ft) + \sqrt{2D}\xi\ (\mathrm{t}) \end{cases} \tag{8}$$

Next, we let $A = 0$, $D = 0$, $\mathrm{d}x/\mathrm{d}t = 0$, $\mathrm{d}y/\mathrm{d}t = 0$. Therefore, we can obtain five singularities of nonlinear systems:

$$\begin{aligned} (x_{2-}, y_{2-}) &= (-\sqrt{\frac{-c-k}{2d}}, 0) \\ (x_{1-}, y_{1-}) &= (-\sqrt{\frac{-c+k}{2d}}, 0) \\ (x_0, y_0) &= (0, 0) \\ (x_{1+}, y_{1+}) &= (\sqrt{\frac{-c+k}{2d}}, 0) \\ (x_{2+}, y_{2+}) &= (\sqrt{\frac{-c-k}{2d}}, 0). \end{aligned}$$

where $\sqrt{c^2 - 4bd} = k$.

After deducing the Fokker-Planck equation, the probability density function of particle motion can be shown as follows:

$$\begin{aligned} &\frac{\partial}{\partial t}\rho(x, y, t) \\ &\quad = -\frac{\partial}{\partial x}[y\rho(x, y, t)] \\ &\qquad - \frac{\partial}{\partial y}\left[(-bx - cx^3 - dx^5 + A\cos(\Omega t))\rho(x, y, t)\right] \\ &\qquad + D(\frac{\partial}{\partial x^2} + \frac{\partial}{\partial y^2})\rho(x, y, t) \end{aligned} \tag{9}$$

Subsequently, according to adiabatic theory, the quasi-steady-state distribution function of Eq. (9) can be defined as:

$$\mathrm{P}_{st}(x, y, t) = N\exp(-\frac{\tilde{U}(x, y, t)}{D}) \tag{10}$$

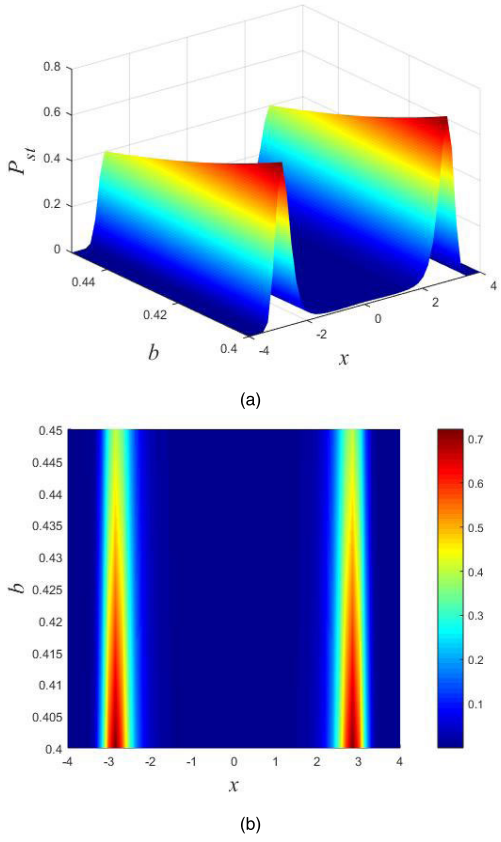

FIGURE 4. (a) The stationary probability. (b) The contour of stationary probability as a function of versus x and different values b with $c = -0.46$, $d = 0.05$, $D = 0.35$.

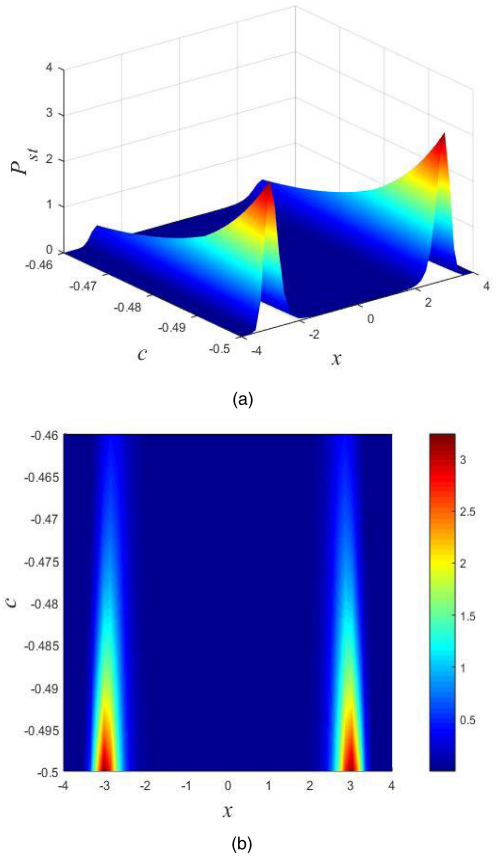

FIGURE 5. (a) The stationary probability. (b) The contour of stationary probability as a function of versus x and different values c with $b = 0.45$, $d = 0.05$, $D = 0.35$.

where N represents the normalization constant, and $\tilde{U}(x, y, t)$ is generalized potential function based on underdamped multistable stochastic resonance system, which can be obtained as:

$$\tilde{U}(x, y, t) = \frac{b}{2}x^2 + \frac{c}{4}x^4 + \frac{d}{6}x^6 + \frac{1}{2}y^2 - xA\cos(\Omega t) \quad (11)$$

The steady state probability density function is the important physical quantity of the nonlinear dynamic system. The noise induced phase transition is an important phenomenon in the random dynamics. Therefore, we study the steady state probability density evolution based on the multistable underdamped system under Gaussian white noise. Fig. 4, 5, 6, and 7 respectively analyze the effects of system parameters b, c, d and noise intensity D on the steady-state probability density function. We can observe that the steady-state probability density of the particle is closely related to the position of the well in which it is located. When the particle is in the middle of the potential well, the particle is in the most stable state. As the system parameters b, c, and d change, the potential well changes, resulting in a change in the steady-state probability density.

Subsequently, according to the theory of adiabatic elimination, the probability transfer rate of particles between potential wells can be written as:

$$R_1(t) = \frac{|U''(-x_1)\,U''(-x_2)|^{1/2}}{2\pi}\exp\left\{-\frac{\tilde{U}(-x_1, -y_1, t) - \tilde{U}(-x_2, -y_2, t)}{D}\right\} \quad (12)$$

$$R_2(t) = \frac{|U''(x_1)\,U''(x_2)|^{1/2}}{2\pi}\exp\left\{-\frac{\tilde{U}(x_1, y_1, t) - \tilde{U}(x_2, y_2, t)}{D}\right\} \quad (13)$$

Make $x_1 = 0, x_0 = -\sqrt{\frac{-c+k}{2d}}, x_2 = \sqrt{\frac{-c-k}{2d}} - \sqrt{\frac{-c+k}{2d}}$

$$\begin{aligned} R_0 &= 2R_1(t)|_{A\cos(\Omega)t=0} \\ &= \frac{b^2 - 3bc^2d - 3bc\sqrt{(c^2-k^2)}d^2 + 5b\left(2c^2-k^2\right)d - 10bc\sqrt{(c^2-k^2)}d^2}{\pi} \\ &\quad \exp\left(\frac{bg2 + cg^24 + dg^36}{D}\right) \\ \frac{1}{2}R_1 &= -\frac{dR_1(t)}{d(A\cos(\Omega t))}|_{\cos(\Omega t)=0} \\ R_1\beta &= \frac{R_0A(x_2 - x_1)}{D} \end{aligned} \quad (14)$$

where $g = -\frac{c}{d} - \sqrt{\frac{c^2-k^2}{d^2}}$

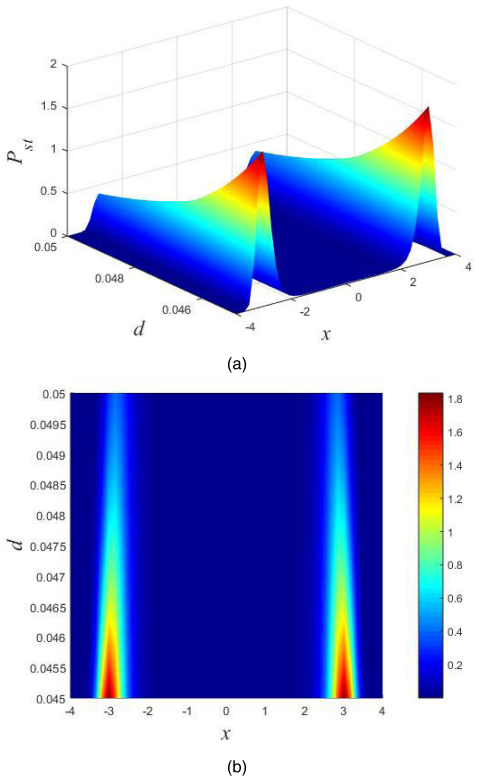

FIGURE 6. (a) The stationary probability. (b) The contour of stationary probability as a function of versus x and different values d with $b = 0.45$, $c = -0.46$, $D = 0.35$.

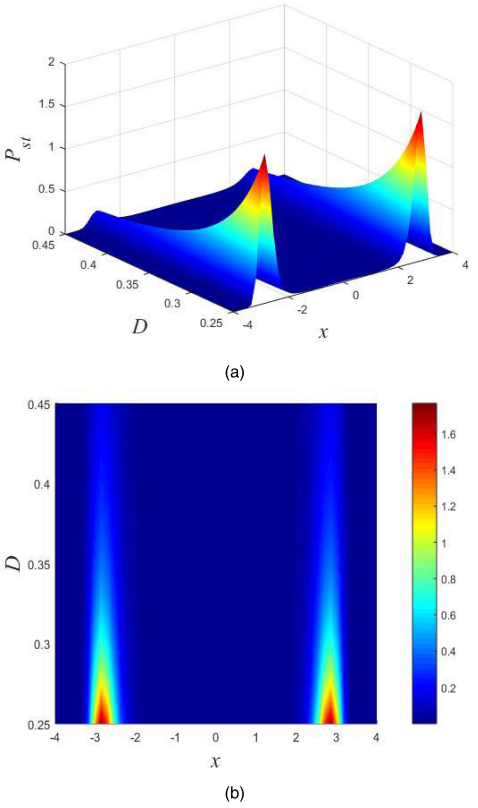

FIGURE 7. (a) The stationary probability. (b) The contour of stationary probability as a function of versus x and different values D with $b = 0.45$, $c = -0.46$, $d = 0.05$.

The output power spectrum of the system is as follows:

$$S(\omega) = S_1(\omega) + S_2(\omega) \tag{15}$$

$S_1(\omega)$ and $S_2(\omega)$ are power spectra of signal and noise, which can be written as:

$$S_1(\omega) = \left(\frac{-c}{8d} - \frac{1}{4}\sqrt{\frac{b}{d}} - \frac{c+k}{8d}\right) \cdot \frac{\pi R_1^2 \beta^2}{2\left(R_0^2 + \Omega^2\right)}[\delta(\omega - \Omega) + \delta(\omega + \Omega)] \tag{16}$$

$$S_2(\omega) = \left(\frac{-c}{8d} + \frac{1}{4}\sqrt{\frac{b}{d}} - \frac{c+k}{8d}\right) \cdot \frac{2R_0}{R_0^2 + \omega^2} \tag{17}$$

The output signal-to-noise ratio of the system can be deduced as:

$$\mathrm{SNR} = \frac{\int_0^\infty S_1(\omega)\, d\omega}{S_2(\omega = \Omega)} = \frac{-\frac{1}{8}\left(\frac{c}{d} + 2\sqrt{\frac{b}{d}}\right) - \frac{k+c}{8d}}{\frac{1}{8}\left(\frac{c}{d} + 2\sqrt{\frac{b}{d}}\right) - \frac{k+c}{8d}} \cdot \frac{\pi R_0 A^2}{4D^2}\left(\frac{-c}{d} - 2\sqrt{\frac{b}{d}}\right) \tag{18}$$

Fig. 8 shows the output SNR of several different stochastic resonance systems as a function of noise intensity. As can be seen, the signal-to-noise ratio is first enhanced as the noise increases, reaching the maximum value, and finally decreasing. However, the signal-to-noise ratio peaks and the optimal noise corresponding to each model are different. As can be seen from the figure, the SUTSR system has strong noise transfer capability compared to other systems.

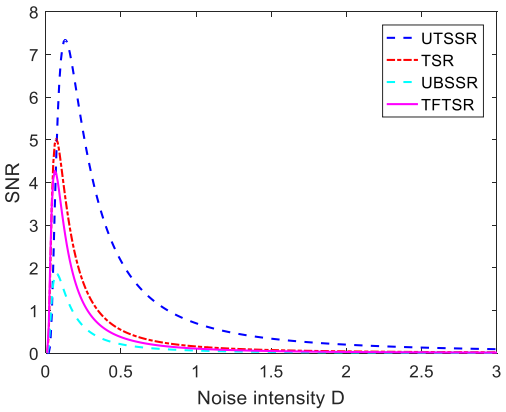

FIGURE 8. The output SNR with noise intensity.

In this section, under the small parameters and combined with progressive elimination theory's condition, the output SNR of the second order stochastic resonance model based on multi-steady state is deduced. It can be seen from Fig.8, Fig.9 and Fig.10 that non-monotonic change in SNR indicates the presence of stochastic resonance phenomenon of

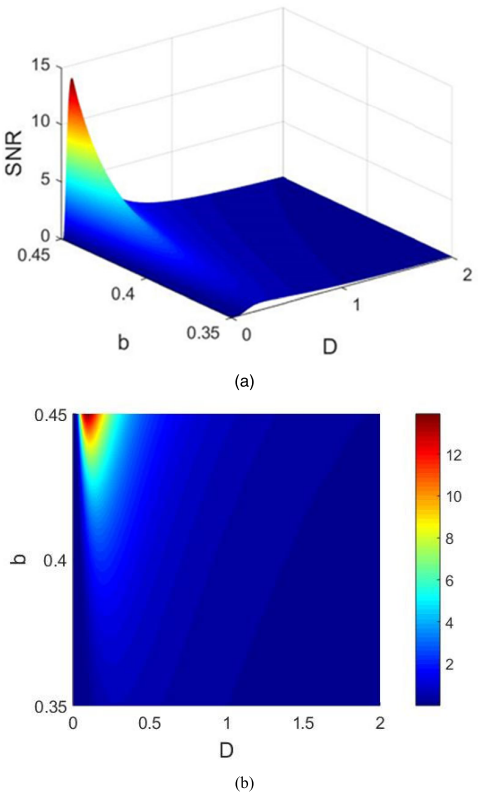

FIGURE 9. (a) SNR. (b) The contour of SNR as a function of the noise intensity D and the system parameter b with $c = -0.46$, $d = 0.05$, $A = 0.2$.

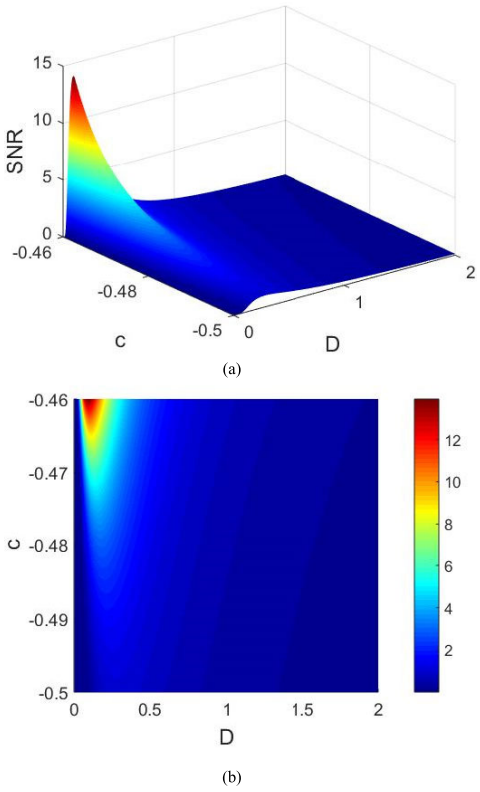

FIGURE 10. (a) SNR. (b) The contour of SNR as a function of the noise intensity D and the system parameter c with $b = 0.45$, $d = 0.05$, $A = 0.2$.

nonlinear systems. Fig. 9 shows the change trends of SNR and its contour as a function of noise intensity D and the system parameters b with $c = -0.46$, $d = 0.05$, $A = 0.2$. When $0.35 < b < 0.45$, first, the SNR increases with the increase of D, after the maximum value is reached, it decreases with the increase of D. At the same time, with the increases of b, the peak value of the SNR begins to increase and the position of the peak shifts to the left. When $b = 0.45$, the SNR reaches the maximum value of 13.91. Fig.10 shows the SNR's change trends and its contour as a function of noise intensity D and the system parameters c with $b = 0.45$, $d = 0.05$, $A = 0.2$ and Fig.11 shows the change trends of SNR and its contour as a function of noise intensity D and the system parameters d with $b = 0.45$, $c = -0.46$, $A = 0.2$. We found that the SNR functions of the parameter b, c within a certain range trends are very similar. The peak value of the SNR increases with the increase of system parameter b and c. Meanwhile, the peak is shifted to the left by the noise intensity D. Therefore, when we use this model to extract weak signal features, we must fully consider the influence of parameters on the system.

III. OUTPUT RESPONCE OF THE SUTSR SYSTEM

A. DYNAMIC RESPONSE ANALYSIS BASD ON STEAD-STATE SOLUTIONCURVE

When it has a steady input case, the system equation of constant excitation can be obtained from Eq. (7) as follows:

$$\frac{\mathrm{d}^2x}{\mathrm{d}t^2} + \gamma\frac{\mathrm{d}x}{\mathrm{d}t} + b\mathrm{x} + cx^3 + dx^5 = h \tag{19}$$

The dynamic equation in state space can be defined as:

$$\begin{cases} \dfrac{\mathrm{d}x}{\mathrm{d}t} = y \\ \dfrac{\mathrm{d}y}{\mathrm{d}t} = -\gamma\mathrm{y} - b\mathrm{x} - cx^3 - dx^5 + h \end{cases} \tag{20}$$

From the perspective of Brownian particle motion, the steady-state response of Eq. (12) means that the velocity and acceleration of Brownian motion are both zero.

$$\begin{cases} \dfrac{\mathrm{d}x}{\mathrm{d}t} = y = 0 \\ \dfrac{\mathrm{d}y}{\mathrm{d}t} = -\gamma\mathrm{y} - b\mathrm{x} - cx^3 - dx^5 + h = 0 \end{cases} \tag{21}$$

Equivalent to

$$\begin{cases} -b\mathrm{x} - cx^3 - dx^5 + h = 0 \\ \mathrm{y} = 0 \end{cases} \tag{22}$$

This shows the steady state solution of the system Eq. (7) is equivalent to the solution of Eq. (22), so the implicit expression of the steady-state solution of the system equation as follows:

$$-b\mathrm{x} - cx^3 - dx^5 + h = 0 \tag{23}$$

At the same time, the potential function of the system equation modulated by the constant r is

$$V(x) = \frac{b}{2}x^2 + \frac{c}{4}x^4 + \frac{d}{6}x^6 - hx \tag{24}$$

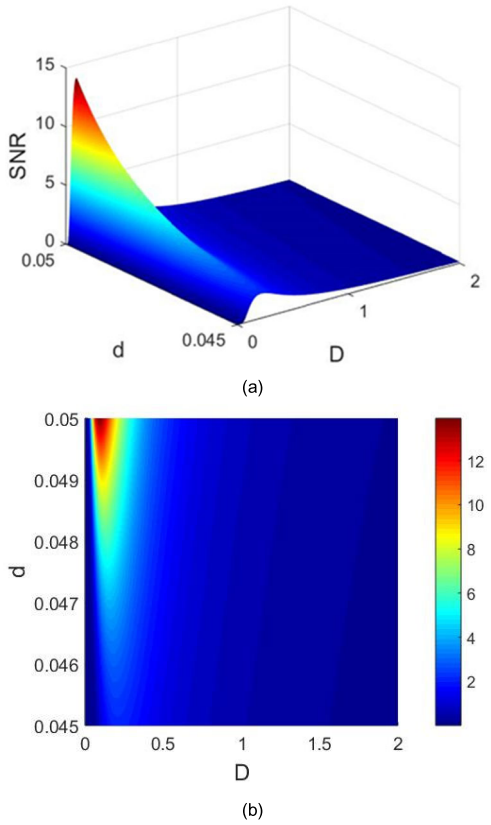

FIGURE 11. (a) SNR. (b) The contour of SNR as a function of the noise intensity D and the system parameter d with $b = 0.45$, $c = -0.46$, $A = 0.2$.

It is not difficult to find that Eq. (24) is equivalent to $\mathrm{d}V(x)/\mathrm{d}x = 0$.

Fig. 12 plots the potential function $u(x)$ before the constant-state system is modulated by the constant r and the potential function $V(x)$ after modulation, at this time $h = 0.5$. At this point, the minimum point of $u(x)$ is $x_{s1,s2,s3}$ and the maximum point of $u(x)$ is x_{u1} and x_{u2}. Due to the constant r modulation, the extreme point of $V(x)$ also changes. Under this parameter condition, it can be seen that $V(x)$ still has three minimum points $(x'_{s1}, x'_{s2}, x'_{s3})$ and two maximum points (x'_{u1}, x'_{u2}). Obviously, the abscissa of these extreme points is the solution of Eq. (23), which is the possible form of the output response of the underdamped multi-stable system. Because of the high-order terms in the equation, we use the graphical method to address it. Define the curve:

$$\begin{cases} g_1(\mathrm{x}) = bx + cx^3 + dx^5 \\ g_2(\mathrm{x}) = h \end{cases} \tag{25}$$

Fig. 13 plots curves g1 and g2, and the number setting is the same as Fig. 12. First, $g_1(x)$ is equal to the derivative $\mathrm{d}u(x)/\mathrm{d}x$ of the potential function $u(x)$. The abscissa values of the five intersections of $g_1(x)$ and the x-axis correspond to the positions of the five extreme points of $u(x)$. Meanwhile, the abscissa value of the intersection of $g_1(x)$ and $g_2(x)$ is the solution of Eq. (23). This solution is also the position of

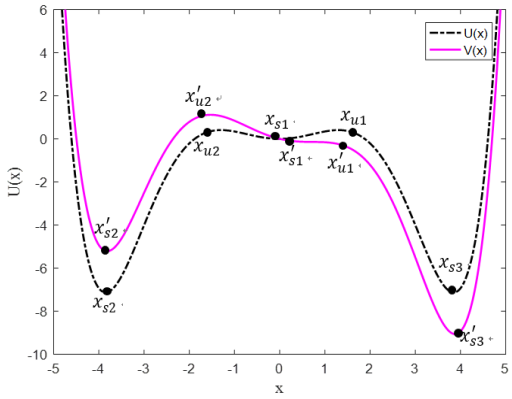

FIGURE 12. The system is modulated by the constant h before and after the modulation of the potential function.

the extreme point of $V(x)$ in Fig. 12, and is also a possible form of the response solution of the SUTSR system Eq. (19). Among the five intersections of $g_1(x)$ and $g_2(x)$, x'_{u1} and x'_{u2} correspond to the maximum points of the potential function $V(x)$, which are also its unstable points. Brownian particles deviate from this equilibrium point under any slight perturbation, so these points are the unsteady solutions of the system. Only the abscissa x'_{s1}, x'_{s2} and x'_{s3} of the intersection of the curves at the middle and the sides are the steady-state solution of the Eq. (19).

Obviously, the number of intersections of curves $g_1(x)$ and $g_2(x)$ is related to the value of r. Deriving the function $g_1(x)$:

$$\frac{\mathrm{d}g_1(x)}{\mathrm{dx}} = b + 3cx^2 + 5dx^4 \tag{26}$$

The four extreme point positions of the solution curve $g_1(x)$ are:

$$\begin{cases} x_{1,2} = \pm\sqrt{\dfrac{-6c - \sqrt{9c^2 - 20bd}}{10d}} \\ x_{3,4} = \pm\sqrt{\dfrac{-6c + \sqrt{9c^2 - 20bd}}{10d}} \end{cases} \tag{27}$$

Among them, x_1 and x_2 represent the two extreme point abscissas closer to the origin, and x_3 and x_4 represent the two extreme point abscissas farther from the origin. Define the extreme point coordinate values of $g_1(x)$:

$$\begin{cases} l_1 = g_1(x_1) \\ l_2 = g_1(x_4) \end{cases} \tag{28}$$

l_1 and l_2 are the two critical values of the constant h. Assume the $l_1 < l_2$, the intersection of the curves $g_1(x)$ and $g_2(x)$ and the change of the potential function can be summarized as Table 1.

Based on the above analysis, we define the curve $g(x)$ as the steady state solution curve of the tristable system equation. Therefore, for a steady-state multi-stable system equation, the output response of the input of the system is a stable intersection of the steady-state solution curve $g_1(x)$ and the input amount curve $g_2(x)$.

TABLE 1. The intersection numbers of $g_1(x)$ and $g_2(x)$, the potential structure form of $V(x)$ and their relationships with invariable r.

	$\|h\| < l_1$	$\|h\| = l_1$	$l_1 < \|h\| < l_2$	$\|h\| = l_2$	$\|h\| > l_2$
Intersection of curves	5	4	3	2	1
Potential function structure of $V(x)$	tristable	double	double	monostable	monostable

B. DYNAMIC RESPONSE ANALYSIS OF BASED ON STEAD-STATE SOLUTIONCURVE

In Eq. (7), let $D = 0$, consider the underdamped multi-stable system of harmonic signal input:

$$\frac{\mathrm{d}^2x}{\mathrm{d}t^2} = -bx - cx^3 - dx^5 - \gamma\frac{\mathrm{d}x}{\mathrm{d}t} + A\cos(2\pi ft + \varphi) \quad (29)$$

When f is small enough, the input of the system is a very slow harmonic signal. When $t = t_p$, $h = \mathrm{sn}(t_p)$. Therefore, the output response of the system is at a stable intersection of the input quantity curve $g_2(x) = \mathrm{sn}(t_p)$ and $g_1(\mathrm{x}) = bx + cx^3 + dx^5$. If an infinite number of steady-state solution x_s is connected in the order of time t, the output response solution of Eq. (17) can be obtained.

We use Eq. (4) Runge-Kutta to solve Eq. (30). The simulation results are shown in Fig. 13. Let e = 0.4, b = 0.45, c = −0.47, d = 0.5 and f_0 = 0.1HZ. Set the initial value of the input signal $x_0 = x_1 = 0$. When A = 0.1, the input signal of the system (Fig. 14 (b)) and the output response map (Fig. 14 (c)) can establish a one-to-one mapping relationship through the steady state solution curve (Fig. 14 (a)).

The abscissa in Fig. 14(b) is the amplitude of the input signal, which corresponds to the curve $g_2(x)$ of Fig. 14(a). As shown in Fig. 12, the initial time system output is at the steady state solution x'_{s1}. In the first quarter cycle, the input signal gradually increases, which is equivalent to the $g_2(x)$ curve in Fig. 14(a) moving to the left, while the steady-state point x'_{s1} increases along the curve $g_1(x)$, so the output of the system gradually increases. When $g_2(x) = A$, the input signal amplitude reaches the maximum, and the output signal is also at the maximum value. Then, in the second quarter cycle, the input signal gradually becomes smaller, equivalent to $g_2(x)$ moving to the right. Currently, the steady-state point x'_{s1} gradually decreases along the curve $g_1(x)$, so the output of the system gradually decreases. When $g_2(x) = 0$, the output becomes 0. Similarly, in the third quarter and the fourth quarter cycle, the system input signal first increases and then decreases, curve $g_2(x)$ move right first to $g_2(x) = -A$, then move left to $g_2(x) = 0$. At this point, the steady-state point increases first and then decreases. Similarly, the output response of the system is also increased to its maximum value and then reduced to zero. Between the extreme positions of the intersection of $g_1(x)$ and $g_2(x)$, a small amplitude oscillation is achieved between the potential wells, and its oscillation period coincides with the period of the input signal.

$$\begin{cases} y_1 = y[n]; \\ x_1 = -U'(x[n]) - \gamma y_1 + S[n] \\ \quad\quad + N[n]; \\ y_2 = y[n] + \dfrac{x_1 h}{2}; \\ x_2 = -U'\left(x[n] + \dfrac{y_1 h}{2}\right) - \gamma y_2 \\ \quad\quad + S[n] + N[n]; \\ y_3 = y[n] + \dfrac{x_2 h}{2}; \\ x_3 = -U'\left(x[n] + \dfrac{y_2 h}{2}\right) - \gamma y_3 \\ \quad\quad + S[n+1] + N[n+1]; \\ y_4 = y[n] + x_3 h; \\ x_4 = -U'\left(x[n] + \dfrac{y_3 h}{2}\right) - \gamma y_4 \\ \quad\quad + S[n+1] + N[n+1]; \\ y[n+1] = y[n] \\ \quad\quad + \dfrac{x_1 + 2x_2 + 2x_3 + x_4}{6}; \\ x[n+1] = x[n] \\ \quad\quad + \dfrac{y_1 + 2y_2 + 2y_3 + y_4}{6}; \end{cases} \quad (30)$$

IV. ENGINEERING APPLICATION

A set of bearing inner ring fault data come from CWRU and bearing roller fault data collected by our own experimental platform to examine the SUTSR model. In the first example, the paper compares the second-order underdamped multi-stability model with the traditional multi-stable stochastic resonance system in fault feature extraction. In the second example, the paper compares the SUTSR method with the second-order underdamped bistable stochastic resonance (SUBSR) to extract weak signal in strong noise background.

A. BEARING INNER RACEWAY FAULT DETECTION

The data for this study comes from the CWRU Bearing Data Center website [36]. Fig. 15 and Fig. 16 are the experimental platform composition diagrams. The drive end bearing model

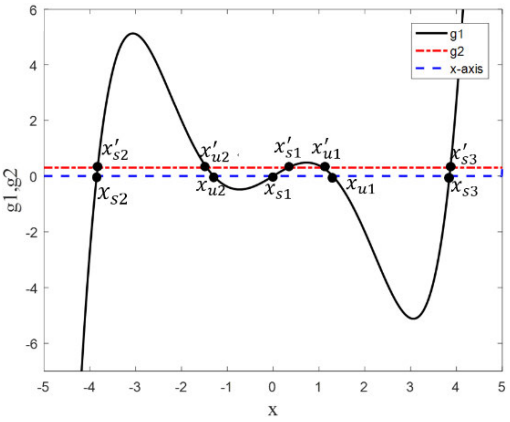

FIGURE 13. Schematic diagram of solving system output response.

is the 6205-2RS type JEM SKF deep groove ball bearing. The spindle speed is 1730 r/min and the sampling frequency is 12 kHz. The bearing parameters are shown in Table 2. After calculation, the characteristic frequency of the bearing inner ring failure is 156.14 Hz.

Fig. 17 shows the time domain diagram and its frequency domain diagram. An obvious periodic shock signal caused by the fault can be seen from the time domain diagram. Very strong high-frequency signal interference can be observed from the Fig.17 (b), and their frequency components are mainly concentrated in 0-2 kHz. The characteristic frequency of the fault signal is flooded by noise. Since the characteristic frequency cannot be directly read from the spectrogram, the paper uses the SR system to extract the fault signal.

In this part, we verify the feasibility of the SUTSR system in fault signal extraction with actual data. At the same time, the processing results are compared with the TSR system. Fig. 18(a) and (b) show the result of processing by the multi-stable stochastic resonance system. It can be observed that the time domain signal impact component is more obvious, but it is still interfered by some noise components. In Fig. 18(b), it can be observed that the amplitude of the signal of 156 Hz is amplified and higher than the amplitude of the other frequencies. It is very similar to 156.14 Hz, which is the theoretical value, so the fault signal is detected after the TSR system. The frequency of the characteristic signal is emphasized, and a periodic signal with a clear principal component has been obtained in the time domain diagram. At the same time, the fault signal is clearly seen in the power spectrum, there is almost no interference of other noise signals. Since the noise energy is transferred to the characteristic signal through the SR system, the amplitude of the signal with a frequency of 156 Hz is greatly improved to 0.7827. This is 0.4259 higher than the characteristic signal amplitude of 0.3532 processed by the TSR system. This is enough to show that the SUTSR system has better noise suppression and weak periodic signal enhancement than the TSR system.

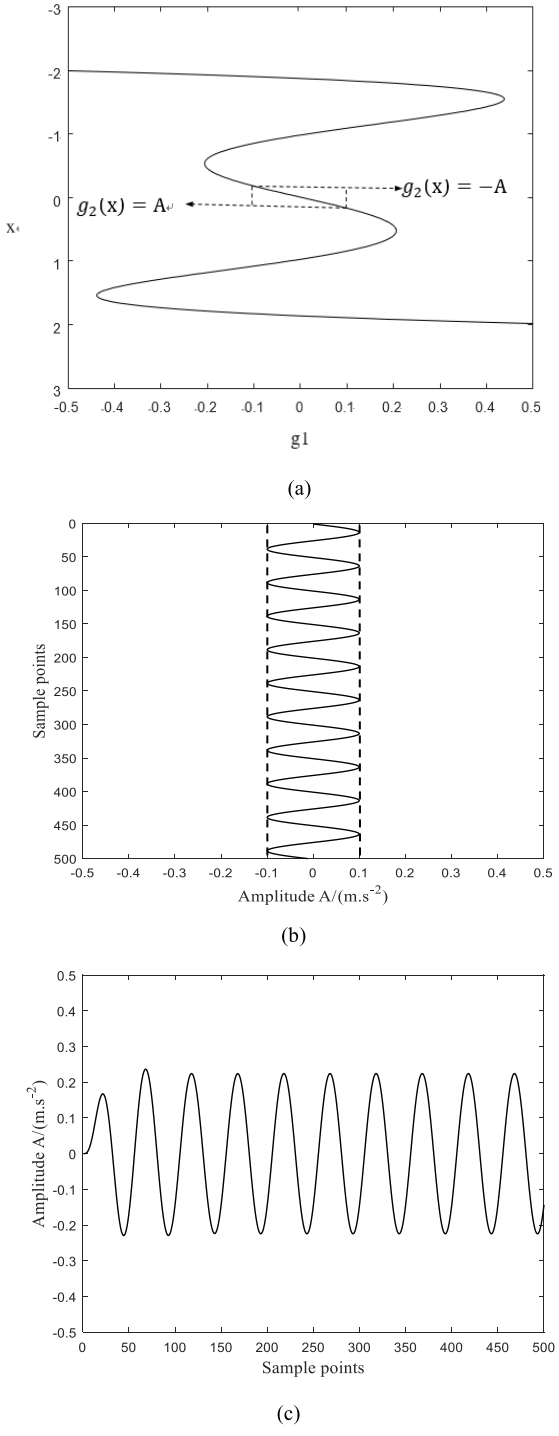

FIGURE 14. System output response map based on steady state solution curve. (a) Steady state solution curve. (b) System input signal. (c) System out signal.

B. BEARING ROLLING ELEMENT FAULT DETECTION

To deeply verify the efficiency of the algorithm, this section tests a test platform with faulty bearings. Fig. 19 shows the test bench. The bearing type is cylindrical roller bearing, model NU205EM. The bearing ball is faulty and the faulty bearing is at the load end. The parameters of the bearing

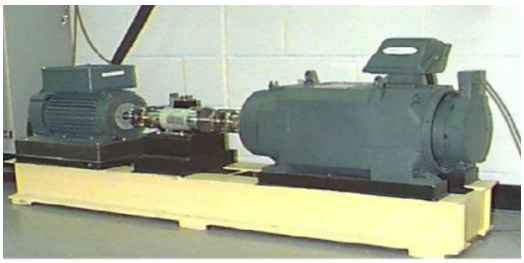

FIGURE 15. Experiment platform.

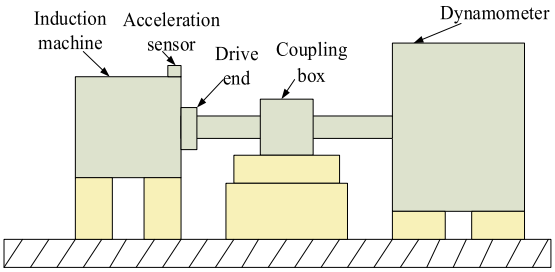

FIGURE 16. Experimental platform composition diagram.

TABLE 2. The main parameters of the rolling bearings.

Name	Value
Inner diameter/ mm	25.001
Outer diameter/ mm	51.999
Pitch diameter/ mm	39.040
Ball diameter/ mm	7.940
Ball number	9.000
Contact angle/(°)	0

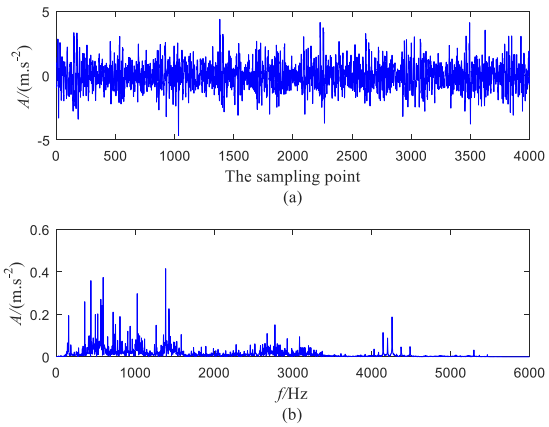

FIGURE 17. Waveform (a) and spectra (b) of a bearing inner ring fault signal.

are shown in Table 3. In this experiment, the motor speed is 1500 r/min and the sampling frequency is 3000 Hz. The theoretical value of the ball fault of the bearing is 82.28 Hz.

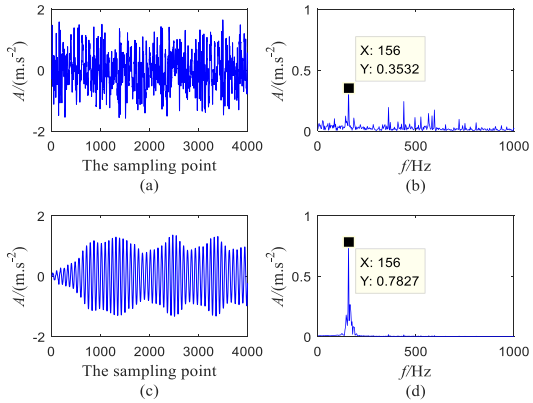

FIGURE 18. Analyzed results by different methods: (a) and (b) optimal output of traditional TSR at $b = 0.45$, $b = -0.65$, $d = 0.38$; (c) and (d) optimal output of SUTSR at $h = 0.05$, $\gamma = 0.04$ $b = 3.83$, $c = -0.25$, $d = 0.75$.

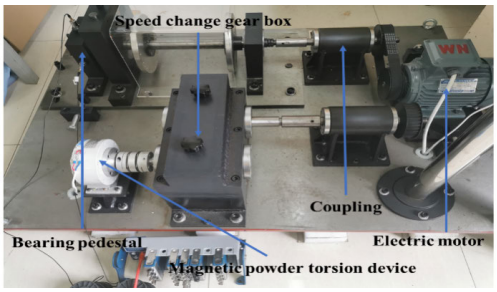

FIGURE 19. Experiment platform.

TABLE 3. The main parameters of the rolling bearings.

Name	Value
Inner diameter/ mm	24.7
Outer diameter/ mm	44.7
Pitch diameter/ mm	45.1
Ball diameter/ mm	6.7
Ball number	13.0
Contact angle/(°)	0

The waveform and its spectrum of the bearing ball fault signal are shown in Fig. 21. Obvious periodic modulation signals are observed from the time domain diagram, but this is not an impact signal caused by rolling element failure. From Fig. 21(b), it can be deduced that the vibration signal is modulated by the frequency of the main shaft (24.75 Hz), and the characteristic signal is submerged. At the same time, the strength of the fault signal is very weak, and the amplitude is 0.008. The frequency conversion and its multiplication, as well as the noise signal, are very strong. Therefore, this section uses SUTSR and second-order underdamped bistable stochastic resonance (SUBSR) systems to process the data.

FIGURE 20. Rolling element failure.

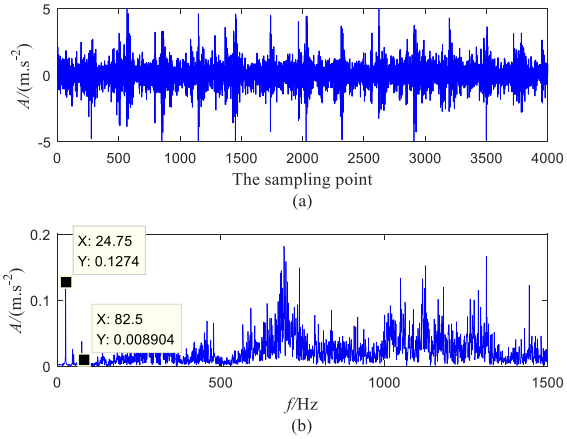

FIGURE 21. Waveform (a) and spectra (b) of a bearing ball fault signal.

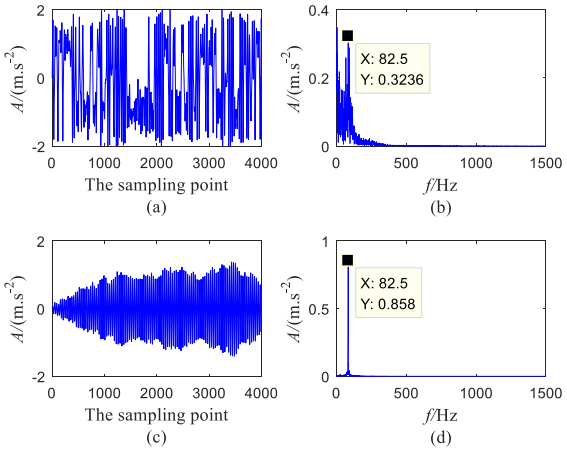

FIGURE 22. Analyzed results of the inner raceway defective signals by using different methods: (a) and (b) optimal output of traditional USBSR at $\gamma = 0.14$, h = 0.17, b = 1, c = 0.9; (c) and (d) optimal output of SUTSR method at h = 0.01, $\gamma = 0.04$ b = 8.83, c = −0.05, d = 0.18.

Fig. 22 (b) and (d) show the frequency domain distribution of the signal after processing by the SR system. The detected signal characteristic frequency is 82.5 Hz. This is very close to 82.28 Hz, which is the theoretical value. Simultaneous observation of Fig. 22 (a) and (c) show that the signal noise is drastically reduced and the periodicity is more prominent. Fig. 22(c) and (d) show the results of the fault signal extracted by the SUBSR and SUTSR method. Obviously, the fault signal is well detected by the SUTSR system. The optimal output signal of the system has almost no noise interference from other frequency components. The time domain signal shows significant periodic fluctuations. By comparing Fig. 22(b) and (d), both methods can complete the extraction work of the weak fault signal, but the filtering effect of the SUTSR system is more obvious, which means that more noise energy to the signal can be transferred. The fault frequency amplitude increases from 0.3236 to 0.858. This result shows that the SUTSR system is more effective for bearing fault feature extraction in the background of strong noise.

Therefore, the proposed SUTSR system can extract the weak fault signal under strong noise background more effectively comparing with the traditional multi-stationary stochastic resonance system and the underdamped second-order bistable stochastic resonance system.

V. CONCLUSION

Considering the secondary filtering effect of underdamped nonlinear systems and the classical stochastic resonance are often using overdamped first-order stochastic differential equations, this paper studies the SUTSR model and its application in fault diagnosis. From the previous analysis, some conclusions can be listed as follows:

1. The effective potential function and steady-state probability density function of the system are deduced and the influences of system parameters are discussed.
2. The output SNR of the SUTSR system is derived and the effect of the parameters b, c and d are discussed. At the same time, the SUTSR system is compared with the output SNR simulation results of several common systems. It can be deduced that the SUTSR system has obvious advantages in improving SNR.
3. The steady-state solution curve is used to discuss the output response of the SUTSR system from the perspective of steady input, and the output response of the system is further studied when the low-frequency harmonic signal is input.
4. The fault bearing signal detection effects of SUTSR, TSR and SUBSR models are compared by actual examples. Analysis shows the SUTSR system performs more accurately and clearly in extracting the characteristic signals. The SNR of the output signal is greatly improved at the same time.

REFERENCES

[1] R. Benzi, A. Sutera, and A. Vulpiani, "The mechanism of stochastic resonance," *J. Phys. A, Math. Gen.*, vol. 14, no. 11, p. L453, Nov. 1981.
[2] R. Benzi, G. Parisi, A. Sutera, and A. Vulpiani, "Stochastic resonance in climatic change," *Tellus*, vol. 34, no. 1, pp. 10–16, Feb. 1982.
[3] S. Fauve and F. Heslot, "Stochastic resonance in a bistable system," *Phys. Lett. A*, vol. 97, nos. 1–2, pp. 5–7, Aug. 1983.
[4] B. Mcnamara, K. Wiesenfeld, and R. Roy, "Observation of stochastic resonance in a ring laser," *Phys. Rev. Lett*, vol. 60, no. 25, pp. 2626–2629, Jun. 1988.
[5] G. Hu, G. Nicolis, and C. Nicolis, "Periodically forced Fokker-Planck equation and stochastic resonance," *Phys. Rev. A, Gen. Phys.*, vol. 42, no. 4, pp. 2030–2041, Aug. 1990.

[6] Z. Hou and H. Xin, "Noise-induced oscillation and stochastic resonance in an autonomous chemical reaction system," *Phys. Rev. E, Stat. Phys. Plasmas Fluids Relat. Interdiscip. Top.*, vol. 60, no. 6, pp. 6329–6332, Dec. 1999.
[7] M. E. Inchiosa and A. R. Bulsara, "Signal detection statistics of stochastic resonators," *Phys. Rev. E, Stat. Phys. Plasmas Fluids Relat. Interdiscip. Top.*, vol. 53, no. 3, pp. 2021–2024, Mar. 1996.
[8] D. Han, P. Li, and S. An, "Multi-frequency weak signal detection based on wavelet transform and parameter compensation band-pass multi-stable stochastic resonance," *Mech. Syst. Signal Process.*, vol. 70, pp. 995–1010, Mar. 2016.
[9] Q. He, E. Wu, and Y. Pan, "Multi-scale stochastic resonance Spectrogram for fault diagnosis of rolling element bearings," *J. Sound Vib.*, vol. 420, pp. 174–184, Apr. 2018.
[10] L. Tong, X. Li, J. Hu, and L. Ren, "A PSO optimization scale-transformation stochastic-resonance algorithm with stability mutation operator," *IEEE Access*, vol. 6, pp. 1167–1176, 2017.
[11] X. Xu, Y. Lei, and Z. Li, "An incorrect data detection method for big data cleaning of machinery condition monitoring," *IEEE Trans. Ind. Electron.*, vol. 67, no. 3, pp. 2326–2336, Mar. 2020.
[12] P. Shi, D. Yuan, D. Han, Y. Zhang, and R. Fu, "Stochastic resonance in a time-delayed feedback tristable system and its application in fault diagnosis," *J. Sound Vib.*, vol. 424, pp. 1–14, Jun. 2018.
[13] Z. Qiao, Y. Lei, J. Lin, and F. Jia, "An adaptive unsaturated bistable stochastic resonance method and its application in mechanical fault diagnosis," *Mech. Syst. Signal Process.*, vol. 84, pp. 731–746, Feb. 2017.
[14] S. Lu, Q. He, and J. Wang, "A review of stochastic resonance in rotating machine fault detection," *Mech. Syst. Signal Process.*, vol. 116, pp. 230–260, Feb. 2019.
[15] S. Lu, Q. He, H. Zhang, and F. Kong, "Enhanced rotating machine fault diagnosis based on time-delayed feedback stochastic resonance," *J. Vib. Acoust*, vol. 137, no. 5, p. 98, Oct. 2015.
[16] L. Gammaitoni, P. Hanggi, P. Jung, and F. Marchesoni "Stochastic resonance," *Rev. Mod. Phys.*, vol. 70, pp. 223–287, Jan. 1998.
[17] Y. Jin, "Noise-induced dynamics in a delayed bistable system with correlated noises," *Phys. A, Stat. Mech. Appl.*, vol. 391, pp. 1928–1933, Mar. 2012.
[18] P. Shi, X. Ding, and D. Han, "Study on multi-frequency weak signal detection method based on stochastic resonance tuning by multi-scale noise," *Measurement*, vol. 47, pp. 540–546, Jan. 2014.
[19] A. Sharma, V. Kohar, M. D. Shrimali, and S. Sinha, "Realizing logic gates with time-delayed synthetic genetic networks," *Nonlinear Dyn.*, vol. 76, no. 1, pp. 431–439, Apr. 2014.
[20] Z. Huo, Y. Zhang, P. Francq, L. Shu, and J. Huang, "Incipient fault diagnosis of roller bearing using optimized wavelet transform based multi-speed vibration signatures," *IEEE Access*, vol. 5, pp. 19442–19456, 2017.
[21] K. Nishiguchi and A. Fujiwara, "Detecting signals buried in noise via nanowire transistors using stochastic resonance," *Appl. Phys. Lett*, vol. 101, no. 19, Nov. 2012, Art. no. 193108.
[22] J. Li, X. Cheng, and Z. Du, "A new noise-controlled second-order enhanced stochastic resonance method with its application in wind turbine drivetrain fault diagnosis," *Renew. Energy*, vol. 3, no. 60, pp. 7–19, Dec. 2013.
[23] Z. Lai and Y. Neng, "Dynamic response and stochastic resonance of a Tri-stable system," *Citation Acta. Phys. Sinica*, vol. 64, Oct. 2015, Art. no. 200503.
[24] Z. Lai and Y. Neng, "Generalized parameter-adjusted stochastic resonance of duffing oscillator and its application to weak-signal detection," *Sensors*, vol. 15, no. 9, pp. 21327–21349, Aug. 2015.
[25] P. Xu, Y. Jin, and Y. Zhang, "Stochastic resonance in an underdamped triple-well potential system," *App. Math. Comput*, vol. 346, pp. 352–362, Apr. 2019.
[26] K. Wang, H. Ye, Y.-J. Wang, and P.-X. Wang, "Impact of time delay and non-gaussian noise on stochastic resonance and stability for a stochastic metapopulation system driven by a multiplicative periodic signal," *Fluct. Noise Lett*, vol. 18, no. 3, Mar. 2019, Art. no. 1950017.
[27] K. Wang, H. Ye, and Y. Wang, "Time-delay-induced dynamical behaviors for an ecological vegetation growth system driven by cross-correlated multiplicative and additive noises," *Eur. Phys. J. E*, vol. 41, no. 5, p. 60, May 2018.
[28] D. Huang, J. Yang, D. Zhou, M. A. F. Sanjuán, and H. Liu, "Recovering an unknown signal completely submerged in strong noise by a new stochastic resonance method," *Commun. Nonlinear Sci*, vol. 66, pp. 156–166, Jan. 2018.
[29] X. Liu, H. Liu, J. Yang, G. Litak, G. Cheng, and S. Han, "Improving the bearing fault diagnosis efficiency by the adaptive stochastic resonance in a new nonlinear system," *Mech. Syst. Signal Process.*, vol. 96, pp. 58–76, Nov. 2017.
[30] M. He, W. Xu, Z. Sun, and W. Jia, "Characterizing stochastic resonance in coupled bistable system with Poisson white noises via statistical complexity measures," *Nonlinear Dyn.*, vol. 88, no. 2, pp. 1163–1171, Apr. 2017.
[31] M. He, W. Xu, Z. Sun, and L. Du, "Characterization of stochastic resonance in a bistable system with Poisson white noise using statistical complexity measures," *Commun. Nonlinear Sci.*, vol. 28, pp. 39–49, Nov. 2015.
[32] P. Yan, F. Duan, and F. Chapeau-Blondeau, "Noise enhancement in robust estimation of location," *IEEE Trans. Signal Process.*, vol. 66, no. 8, pp. 1953–1966, Apr. 2018.
[33] S. Lu, Q. He, and F. Kong, "Effects of underdamped step-varying second-order stochastic resonance for weak signal detection," *Digit. Signal Process*, vol. 36, pp. 93–103, Jan. 2015.
[34] H. Dong, H. Wang, X. Shen, Z. Huang, and S. Ma, "Detection of underwater weak signal via matched stochastic resonance," in *Proc. Oceans-Aberdeen*, Jun. 2017, pp. 1–7.
[35] C. He, P. Niu, and R. Yang, "Incipient rolling element bearing weak fault feature extraction based on adaptive second-order stochastic resonance incorporated by mode decomposition," *Measurement*, vol. 145, pp. 687–701, Oct. 2019.
[36] *Bearing Fault Data of Case Western Reserve University*. Accessed: May 2019. [Online]. Available: http://csegroups.case.edu/bearingdatacenter/pages/12k-drive-end-bearing-faut-data

WENYUE ZHANG received the B.S. degree from the School of Mechanical and Precision Instrument Engineering, Xi'an University of Technology, in 2017. He is currently pursuing the M.S. degree with the Yanshan University, Hebei, China. His research interests include weak signal detection and intelligent fault diagnosis technology.

PEIMING SHI received the Ph.D. degree in information science and engineering from Yanshan University, Qinhuangdao, China, in 2009. He is currently a Professor with the Institute of Electrical Engineering, Yanshan University. His current research interests include fault diagnosis and signal processing.

MENGDI LI received the B.S. degree in the measurement and control technology and communication engineering from the Harbin University of Science and Technology, in 2018. She is currently pursuing the M.S. degree with Yanshan University, Hebei, China. Her current research interests include fault signal detection and stochastic resonance.

YONGXU JIAO is currently pursuing the bachelor's degree in instrument science and technology engineering with Yanshan University of Electrical Engineering, Hebei, China. His research interests include weak signal detection and stochastic resonance.

DONGYING HAN received the Ph.D. degree in mechanical engineering from Yanshan University, Qinhuangdao, China, in 2008, where she is currently an Associate Professor with the Institute of Vehicles and Energy. Her current research interests include fault diagnosis and signal processing.